Supplementary information for "Electrical two-qubit gates within a pair of clock-qubit magnetic molecules"

Aman Ullah [ID],[1,2] Ziqi Hu [ID],[1,2] Jesús Cerdá [ID],[1] Juan Aragó [ID],[1,*] and Alejandro Gaita-Ariño [ID][1,†]

[1]*Instituto de Ciencia Molecular (ICMol), Universitat de València, Paterna, Spain*
[2]*These authors contributed equally to this work*
(Dated: October 26, 2022)

CONTENTS

————

* juan.arago@uv.es
† alejandro.gaita@uv.es

Supplementary Note 1.   ENERGY LEVELS OF THE SINGLE HOW$_{10}$ MOLECULE

The spin energy level scheme for HoW$_{10}$ can be described by the following Hamiltonian:

$$\hat{H} = \sum_{k=2,4,6} \sum_{q=-k}^{k} B_k^q \hat{O}_k^q(J) + \hat{J} \cdot A \cdot \hat{I} + \mu_B g_e B_0 \cdot \hat{J} - \mu_N g_N B_0 \cdot \hat{I}, \tag{1}$$

where, B_k^q are the CFPs in Extended Steven Operator ($\hat{O}_k^q$). J and I are the total electronic and nuclear angular momentum, respectively, whereas "A" denotes the isotropic hyperfine interaction. g_e (g_N) and μ_B (μ_N) correspond to the electronic (nuclear) gyromagnetic ratio and Bohr magneton, respectively. For HoW$_{10}$, $J=8$, $I=7/2$ and $A=0.02768$ cm^{-1} (830 MHz) [1], $g_e=1.25$ and $g_N=1.668$. B_0 is the applied magnetic field.

In the ground 16-level electronuclear spin manifold ($|\pm M_J, \pm M_I\rangle$), the levels of a single HoW$_{10}$ molecule correspond to a electronic spin doublet that is hyperfine coupled to a single nuclear spin octuplet. In both cases, the spin resides in the Ho^{3+} ion. This results in 4 CTs, equispaced in terms of magnetic field and of identical transition frequency, always corresponding to transitions between the 8th and 9th levels. Note that, although the levels involved at the CTs are the same (the 8th and 9th levels), they are different in nature due to the multiple crossings in this dense spectrum. Figure 1 displays the energy evolution of the electronuclear states as a function of a B-field applied along the easy axis of the magnetization (B_0z).
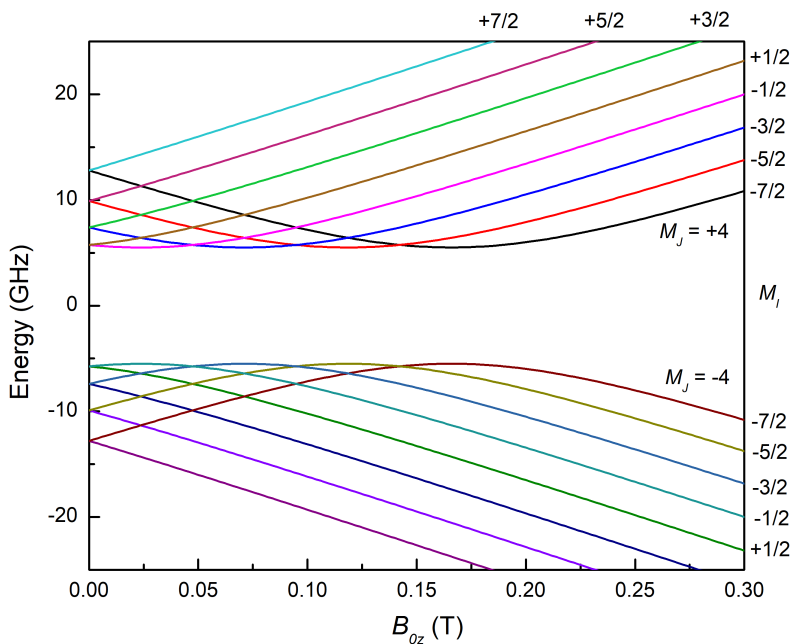
Supplementary Figure 1. Calculated Zeeman diagrams for the 16 states of the $M_J = \pm 4$, $I = 7/2$ electro-nuclear spin ground manifold vs a B-field applied along the easy axis of the magnetization (B_0z). The electronic spin wavefunction varies continuously, with perfect mixing at each CT, as the curve attains zero slope, and pure electronic spin state at effectively infinite distance from the CT. The nuclear spin wavefunction is always pure, since no extradiagonal term acting on the nuclear spin is included in the Hamiltonian.

Supplementary Note 2. RELAXATION DYNAMICS: REDFIELD THEORY

The total Hamiltonian is decomposed in the spin, phonon and spin-phonon Hamiltonians as described in Eqs. 8, 9 and 10 respectively in main text. For convenience, we write Eq. 10 in a more compact way as

$$\hat{H}_{S-ph} = \sum_\alpha \left(\frac{\partial \hat{H}_S}{\partial \hat{q}_\alpha} \right)_0 \hat{q}_\alpha = \sum_\alpha \hat{V}^\alpha \hat{q}_\alpha \tag{2}$$

The dynamics of the total system (electronic spin states + the phonon bath) can be described by the time evolution of density operator $\hat{\rho}$. In interaction picture, this is defined as:

$$\frac{d\hat{\rho}(t)}{dt} = -\frac{i}{\hbar} \left[\hat{H}_{S-ph}(t), \hat{\rho}(t) \right] \tag{3}$$

integral form of Eq. 3 takes the form for time $0 \to$ t as follows:

$$\hat{\rho}(t) = \hat{\rho}(0) - \frac{i}{\hbar} \int_0^t ds \left[\hat{H}_{S-ph}(t), \hat{\rho}(s) \right] \tag{4}$$

By inserting Eq.4 in Eq. 3 and taking trace over phonon bath, this leads to:

$$\frac{d}{dt} \hat{\rho}^s(t) = -\frac{1}{\hbar^2} \int_0^t ds\, tr_B \left[\hat{H}_{S-ph}(t), \left[\hat{H}_{S-ph}(s), \hat{\rho}(s) \right] \right] \tag{5}$$

At this point, we have to make some approximations. First, the coupling between the system (electronic spin states) and phonons is weak and can be treated as a perturbation. Second, the process is Markovian meaning phonon bath relaxation is much faster than the time scale for the spin dynamics. These approximation can be enumerated as,

1. $\hat{\rho}(t) \approx \hat{\rho}^s(t) \otimes \hat{\rho}^B_{eq}$ (weak-couplings, Born-approximation)

2. $\hat{\rho}^s(s) \to \hat{\rho}^s(t)$, $t' = t - s$ (Markov-approximation)

After casting these approximations, the time evolution of the reduced system takes the form:

$$\frac{d}{dt} \hat{\rho}^s(t) = -\frac{1}{\hbar^2} \int_0^\infty dt'\, tr_B \left[\hat{H}_{S-ph}(t), \left[\hat{H}_{S-ph}(t - t'), \hat{\rho}^s(t) \otimes \hat{\rho}^B_{eq} \right] \right] \tag{6}$$

By substituting the definition of $\hat{H}_{S-ph}$ from Eq. 2 into Eq. 6,

$$\frac{d}{dt} \hat{\rho}^s(t) = -\frac{1}{\hbar^2} \int_0^\infty dt'\, tr_B \sum_\alpha \left[\hat{V}^\alpha(t) \hat{q}_{\alpha q}(t), \left[\hat{V}^\alpha(t - t') \hat{q}_\alpha(t - t'), \hat{\rho}^s(t) \otimes \hat{\rho}^B_{eq} \right] \right] \tag{7}$$

After expanding the commutator followed by some mathematical steps, Eq. 7 is expanded as:

$$\frac{d}{dt} \hat{\rho}^s(t) = -\frac{1}{\hbar^2} \int_0^\infty dt' \sum_\alpha \left\{ \right.$$
$$\left[\hat{V}^\alpha(t) \hat{V}^\alpha(t - t') \hat{\rho}^S(t) - \hat{V}^\alpha(t) \hat{\rho}^s(t) \hat{V}^\alpha(t - t') \right] tr_B \left(\hat{q}_\alpha(t) \hat{q}_\alpha(t - t') \hat{\rho}^B_{eq} \right) -$$
$$\left[\hat{V}^\alpha(t - t') \hat{\rho}^s(t) \hat{V}^\alpha(t) - \hat{\rho}^s(t) \hat{V}^\alpha(t) \hat{V}^\alpha(t - t') \right] tr_B \left(\hat{q}_\alpha(t - t') \hat{q}_\alpha(t) \hat{\rho}^B_{eq} \right) \left. \right\} \tag{8}$$

Eq. 8 can be expressed in terms of the eigenstates of $\hat{H}_S$ leading to:

$$\frac{d\rho^s_{ab}(t)}{dt} + i\omega_{ab}\rho^s_{ab} = -\frac{1}{\hbar^2} \int_0^\infty dt' \sum_\alpha \left\{ \right.$$
$$[V^\alpha_{ac}(t) V^\alpha_{cd}(t - t') \rho^s_{db}(t) - V^\alpha_{ac}(t) V^\alpha_{db}(t - t') \rho^s_{cd}(t)] tr_B \left(\hat{q}_\alpha(t) \hat{q}_\alpha(t - t') \hat{\rho}^B_{eq} \right) -$$
$$[V^\alpha_{ac}(t - t') V^\alpha_{db}(t) \rho^s_{cd}(t) - V^\alpha_{cd}(t) V^\alpha_{db}(t - t') \rho^s_{ac}(t)] tr_B \left(\hat{q}_\alpha(t - t') \hat{q}_\alpha(t) \hat{\rho}^B_{eq} \right) \left. \right\} \tag{9}$$

where $\rho_{ab}^s = \langle b| \hat{\rho}^s |a\rangle$ is a reduced system density matrix element and $\omega_{ab} = (E_b - E_a)/\hbar$, being E_b and E_a eigenvalue energies of the spin Hamiltonian.

Explicit time dependencies for the spin-phonon coupling can be described by going back to the Schrödinger picture $V_{ab}^\alpha(t) = \langle a| e^{iH_S t}\hat{V}^\alpha e^{-iH_S t} |b\rangle$,

$$\frac{d\rho_{ab}^s(t)}{dt} + i\omega_{ab}\rho_{ab}^s = -\frac{1}{\hbar^2}\sum_\alpha \left\{ \sum_j \delta_{bd}V_{aj}^\alpha V_{jc}^\alpha \int_0^\infty dt' e^{-i\omega_{jc}t'} tr_B \left(\hat{q}_{\alpha q}(t)\hat{q}_\alpha(t-t')\hat{\rho}_{eq}^B\right) \right.$$

$$- V_{ac}^\alpha V_{db}^\alpha \int_0^\infty dt' e^{-i\omega_{db}t'} tr_B \left(\hat{q}_\alpha(t)\hat{q}_\alpha(t-t')\hat{\rho}_{eq}^B\right)$$

$$- V_{ac}^\alpha V_{db}^\alpha \int_0^\infty dt' e^{-i\omega_{ac}t'} tr_B \left(\hat{q}_\alpha(t-t')\hat{q}_\alpha(t)\hat{\rho}_{eq}^B\right)$$

$$\left. + \sum_j \delta_{ca}V_{dj}^\alpha V_{jb}^\alpha \int_0^\infty dt' e^{-i\omega_{dj}t'} tr_B \left(\hat{q}_\alpha(t-t')\hat{q}_\alpha(t)\hat{\rho}_{eq}^B\right) \right\} \tag{10}$$

The Fourier transformation of the bath correlation function can be written as

$$\int_0^\infty dt' e^{-i\omega_{ij}t'} tr_B \left(\hat{q}_\alpha(t)\hat{q}_\alpha(t-t')\hat{\rho}_B^{eq}\right) = \frac{1}{2}\int_0^\infty dt' e^{-i\omega_{ij}t'} tr_B \left[e^{i\omega_\alpha t'}\hat{a}_\alpha^\dagger \hat{a}_\alpha + e^{-i\omega_\alpha t'}\hat{a}_\alpha\hat{a}_\alpha^\dagger\right]$$

$$= \frac{1}{2}\int_0^\infty dt' e^{-i(\omega_{ij}-\omega_\alpha)t'} \bar{n}_\alpha + \frac{1}{2}\int_0^\infty dt' e^{-i(\omega_{ij}+\omega_\alpha)t'} (\bar{n}_\alpha + 1) \tag{11}$$

where, $\bar{n}_\alpha = tr_B \left[\hat{a}_\alpha^\dagger, \hat{a}_\alpha\right]$ is average phonon number. By using the definition of $\int_0^\infty dt' e^{-i\omega t'} = \pi\delta(\omega)$, Eq. 10 becomes:

$$\frac{d\rho_{ab}^s(t)}{dt} + i\omega_{ab}\rho_{ab}^s = -\frac{\pi}{2\hbar^2}\sum_\alpha \left\{ \sum_j \delta_{bd}V_{aj}^\alpha V_{jc}^\alpha G(\omega_{jc},\omega_\alpha) - V_{ac}^\alpha V_{db}^\alpha G(\omega_{db},\omega_\alpha) \right.$$

$$\left. - V_{ac}^\alpha V_{db}^\alpha G(\omega_{ca},\omega_\alpha) + \sum_j \delta_{ca}V_{dj}^\alpha V_{jb}^\alpha G(\omega_{jd},\omega_\alpha) \right\} \tag{12}$$

where $G(\omega)$ denotes the phonon spectral density, which contains the information of the temperature dependence of spin-dynamics carried by molecular vibrations. Within the harmonic approximation, where phonons are undamped, this is described by dirac-delta function [2, 3],

$$G(\omega_{ij},\omega_\alpha) = \delta(\omega_{ij} - \omega_\alpha)\bar{n}_\alpha + \delta(\omega_{ij} + \omega_\alpha)(\bar{n}_\alpha + 1) \tag{13}$$

The spin-phonon coupling constant expressed in eigenvectors in Eq. 12 can be conveniently written in M_J basis as follows:

$$V_{ab}^\alpha = \sum_\kappa \sum_\lambda \langle a|\kappa\rangle \langle\kappa| \hat{V}^\alpha |\lambda\rangle \langle\lambda|b\rangle \tag{14}$$

Note that the matrix elements in M_J basis (i.e., $|\kappa\rangle \equiv |M_J\rangle$) are the ones directly evaluated by the *ab initio* CASSCF calculations since the spin Hamiltonian $\hat{H}_S$ has been built in these basis.

Finally, Eq. 12 can be written in a more compact and general way:

$$\frac{d\rho_{ab}^s(t)}{dt} = -i\omega_{ab}\rho_{ab}^s - \sum_{c,d} R_{ab,cd}\rho_{cd}^s(t) \tag{15}$$

where, $R_{ab,cd}$ corresponds to the full tetradic RedField tensor. To calculate this tensor, we therefore need to estimate the spin-phonon coupling matrix elements, which were previously calculated from *ab-initio* electronic structure calculations (see Supplementary Table 2 and Ref. [4]), and a expression for the phonon spectral density $G(\omega)$. For the latter, we are using, instead of Eq. 14, the expression proposed by Lunghi et al.[5–8], which is more appropriate for real molecular systems since it incorporates anharmonicity. This spectral density reads as:

$$G(\omega_{ij},\omega_\alpha) = \frac{1}{\pi}\left[\frac{\Delta_\alpha}{\Delta_\alpha^2 + (\omega_{ij} - \omega_\alpha)^2}\bar{n}_\alpha + \frac{\Delta_\alpha}{\Delta_\alpha^2 + (\omega_{ij} + \omega_\alpha)^2}(\bar{n}_\alpha + 1)\right] \tag{16}$$

where, $\bar{n}_\alpha = \frac{1}{e^{\beta\hbar\omega_\alpha}-1}$, is the Bose-Einstein population at a temperature T and $\beta = 1/k_B T$. Δ_α is the Lorentzian vibrational linewidth. Temperature dependence of spectral line-width can be defined as:

$$\Delta_\alpha^2 = \frac{\partial \langle H_{vib,\alpha} \rangle}{\partial \beta} = \frac{(\hbar\omega_\alpha)^2 e^{\beta\hbar\omega_\alpha}}{\left(e^{\beta\hbar\omega_\alpha} - 1\right)^2} \tag{17}$$

where, $\beta = 1/k_B T$, k_B is the boltzman constant.

Supplementary Table 1. Energy level scheme (in cm^{-1}), predominant M_j microstate contribution (10%) and expectation value of total angular momentum $\langle J_z \rangle$ for the ground multiplet of HoW$_{10}$ calculated at CASSCF level on the *crystallographic coordinates*. The atomic coordinates are oriented with the easy axis of magnetization along the z axis.

E$_{CASSCF}$(cm^{-1})	M_J	$\langle J_z \rangle$	E$_{CASSCF}$(cm^{-1})	M_J	$\langle J_z \rangle$
0.00	47.5% $\lvert \pm 4 \rangle$	-5.53	0.36	47.5% $\lvert \pm 4 \rangle$	5.53
26.24	47.2% $\lvert \pm 3 \rangle$	-3.06	27.92	47.2% $\lvert \pm 3 \rangle$	3.06
50.08	48.7% $\lvert \pm 5 \rangle$	-5.31	50.31	48.7% $\lvert \pm 5 \rangle$	5.31
86.70	48.2% $\lvert \pm 2 \rangle$	-2.19	96.34	48.2% $\lvert \pm 2 \rangle$	2.19
155.59	48.9% $\lvert \pm 1 \rangle$	-1.23	156.90	48.9% $\lvert \pm 1 \rangle$	1.23
178.90	46.6% $\lvert \pm 6 \rangle$	-6.36	179.05	46.6% $\lvert \pm 6 \rangle$	6.36
181.88	94.3% $\lvert 0 \rangle$	0.00			
279.97	49.3% $\lvert \pm 8 \rangle$	-9.20	279.97	49.3% $\lvert \pm 8 \rangle$	9.20
315.99	49.1% $\lvert \pm 7 \rangle$	-7.53	315.99	49.1% $\lvert \pm 7 \rangle$	7.53

Supplementary Table 2: Spin-vibrational coupling coefficients - $\sum_{k=2,4,6} \sum_{q=-k}^{k} \left(\frac{\partial B_k^q}{\partial q_\alpha} \right)$ in (cm^{-1}), numerical derivatives are obtained by fitting the evolution of CFPs (B_k^q) along the displacement vector of normal mode-α with second order polynomial.

(k,q)	$\alpha = 68.4$ cm^{-1} $\left(\frac{\partial B_k^q}{\partial q_\alpha} \right)$ (cm^{-1})	$\alpha = 94.5$ cm^{-1} $\left(\frac{\partial B_k^q}{\partial q_\alpha} \right)$ (cm^{-1})	$\alpha = 149.0$ cm^{-1} $\left(\frac{\partial B_k^q}{\partial q_\alpha} \right)$ (cm^{-1})
(2, -2)	-0.04796	0.09267	-0.00031
(2, -1)	0.00172	-0.00505	0.00306
(2, 0)	-0.00369	0.00375	0.00279
(2, 1)	0.16933	-0.30027	-0.00370
(2, 2)	-0.00956	0.01411	-0.01288
(4, -4)	-0.00010	0.00010	0.00013
(4, -3)	-0.00085	-0.00069	-0.00001
(4, -2)	0.00011	-0.00003	0.00016
(4, -1)	-0.00094	-0.00051	0.00000
(4, 0)	-0.00003	-0.00003	-0.00002
(4, 1)	-0.00028	0.00014	-0.00003
(4, 2)	-0.00016	-0.00006	0.00014
(4, 3)	0.00034	-0.00042	-0.00010
(4, 4)	-0.00010	0.00005	-0.00020
(6, -6)	0.00000	-0.00001	0.00000
(6, -5)	-0.00008	-0.00005	0.00000
(6, -4)	0.00000	0.00000	0.00000
(6, -3)	-0.00004	-0.00002	0.00000
(6, -2)	0.00000	0.00000	0.00000
(6, -1)	0.00002	0.00001	0.00000
(6, 0)	0.00000	0.00000	0.00000
(6, 1)	0.00000	0.00001	0.00000
(6, 2)	0.00000	0.00000	0.00000
(6, 3)	0.00000	-0.00001	0.00000
(6, 4)	-0.00001	0.00000	0.00000
(6, 5)	-0.00003	0.00001	0.00000
(6, 6)	0.00000	0.00000	0.00000

Supplementary Note 3.   DETERMINATION OF LONGITUDINAL (T_1) AND TRANSVERSE (T_2) RELAXATION-TIME

To investigate transverse and longitudinal spin relaxation times, T_1 and T_2 respectively. We solved the full RedField theory described in Eq. 15 and 12. From these equation, it is possible to calculate the evolution of a given eigenstate which in turn can be used to calculate the evolution of expected magnetization value:

$$\left\langle \vec{M}(t) \right\rangle = \sum_a \langle a| \rho^s(t)\vec{M} |a\rangle \tag{18}$$

Longitudinal Relaxation time T_1: For the determination of T_1, we prepared the state in system eigenstate of $\hat{H}_s$, $\rho^s(t=0) = |0\rangle \langle 0|$, where $|0\rangle$ represents the lowest eigensate of $\hat{H}_S$. This populated state is then quenched by thermal bath at a given temperature. The decay of the expected magnetization in this process is fitted exponentially as follows:

$$M_z(t) = (M_z(0) - M_z(\infty))e^{-t/\tau} + M_z(\infty) \tag{19}$$

In HoW$_{10}$, the ground state is $|0\rangle = |M_J = -4\rangle$ at CT. Evolution of expected $M_z(t)$ in time is shown in Fig. 2 at 5 and 6 Kelvin.

Transverse Relaxation time T_2:   For the determination of transverse relaxation time T_2, we prepared the initial density in superposition eigenstate of $\hat{H}_s$, $\rho^s(t=0) = |0\rangle \langle 1|$. As indicated above in the description of full Redfield tensor $R_{ab,cd}$, combination of ab,ab will be realized as coherence relaxation. Decay profile is fitted with exponential to obtain the transverse relaxation times.

$$M_{x,y}(t) = (M_{x,y}(0) - M_{x,y}(\infty))e^{-t/\tau} + M_{x,y}(\infty) \tag{20}$$

Coherence relaxation for HoW$_{10}$ is presented in Fig. 3 at 5 and 6 Kelvin.

T_1/T_2 around CT: To determined the T_1/T_2 divergence with magnetic field, we solve the full Redfield tensor at different B-Field around CT, decay profile for expected M_z and $M_{x,y}$ at 5 K is shown in 4 and 5 respectively. In Fig. 6, we show the T_1/T_2 at different B-Field and also at different temperature. Detailed values are provided in Supplementary Table 3 and 4.
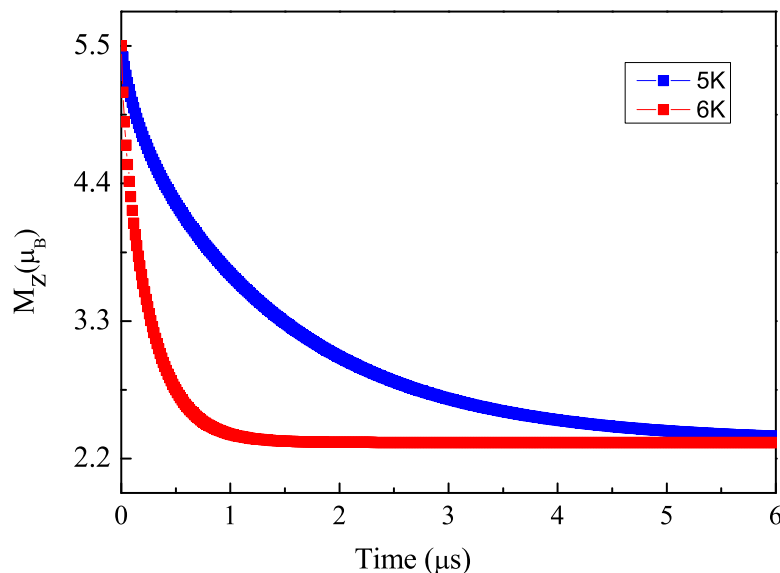
Supplementary Figure 2. Longitudinal (T_1) relaxation-time-temperature dependence at magnetic field of CT.
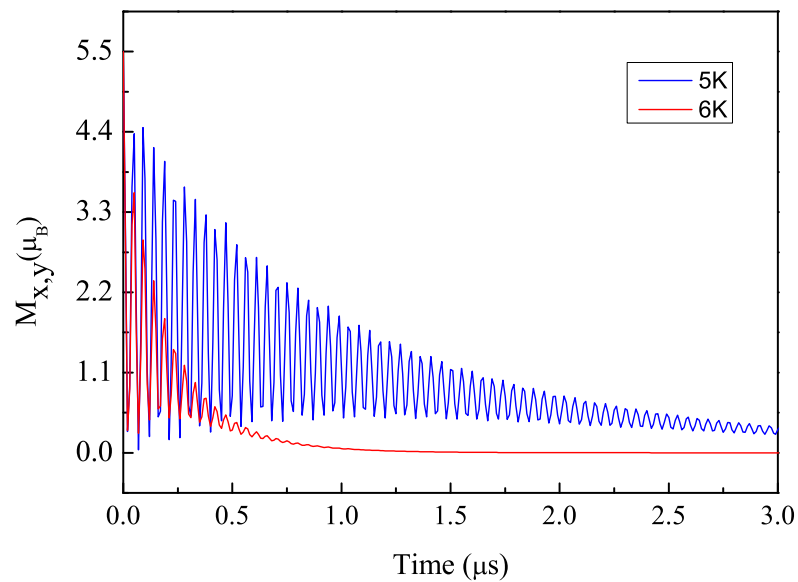
Supplementary Figure 3. Transverse (T_2) relaxation-time-temperature dependence at magnetic field of CT.
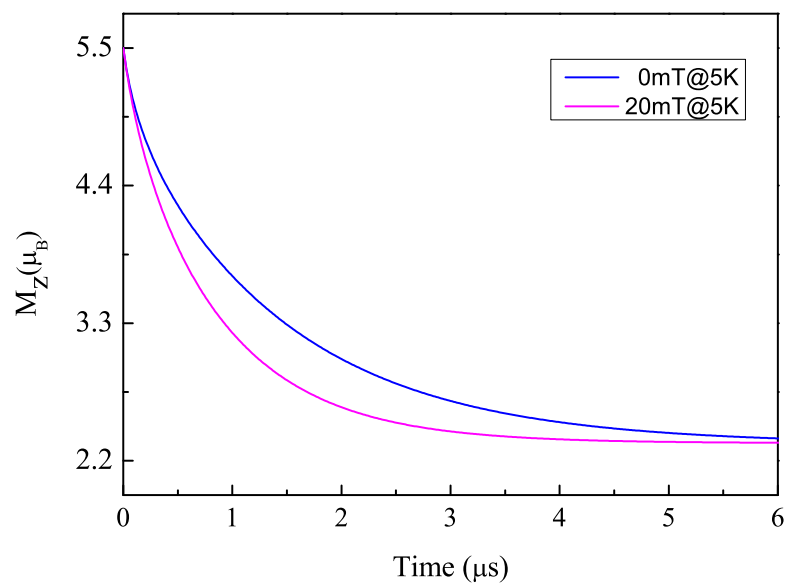
Supplementary Figure 4. Longitudinal (T_1) relaxation at magnetic field of 0 and 20 mT.
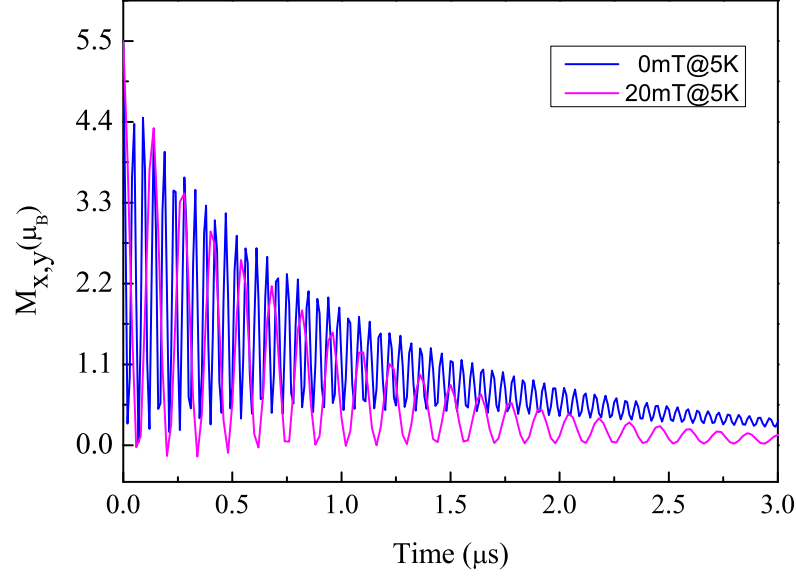
Supplementary Figure 5. Transverse (T_2) relaxation at magnetic field of 0 and 20mT.
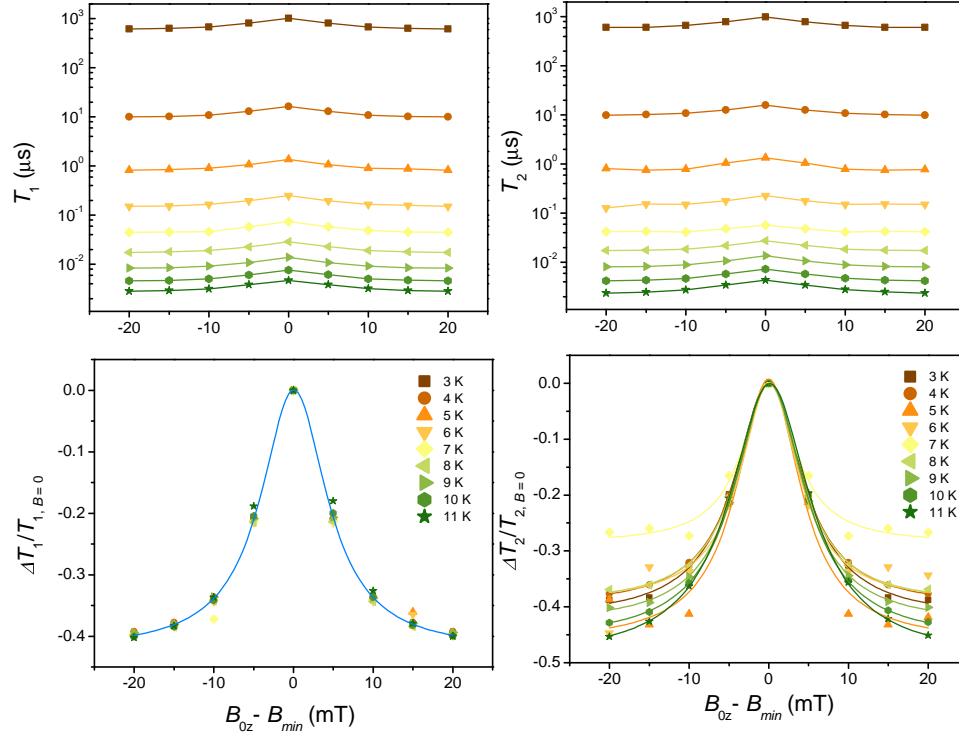
Supplementary Figure 6. a)- Longitudinal (T_1) and b)- transverse (T_2) relaxation-time-temperature dependence at magnetic field of -20 to 20 mT. c)- T_1 and d)- T_2 divergences at CT at different temperatures.

Supplementary Table 3: Longitudinal relaxation time (T_1) in μs at different B-field and different temperatures.

Temperature (K)	-20 mT	-15 mT	-10 mT	-5 mT	0 mT	+5 mT	+10 mT	+15 mT	+20 mT
3	617.843	633.518	676.230	808.439	1026.615	808.440	676.230	633.518	617.842
4	9.999	10.247	10.927	13.028	16.459	13.028	10.927	10.247	9.999
5	0.825	0.845	0.901	1.076	1.363	1.076	0.901	0.872	0.825
6	0.151	0.155	0.165	0.198	0.252	0.198	0.165	0.160	0.151
7	0.045	0.046	0.047	0.058	0.074	0.058	0.049	0.046	0.045
8	0.017	0.018	0.019	0.023	0.029	0.023	0.019	0.018	0.017
9	0.008	0.009	0.009	0.011	0.014	0.011	0.009	0.009	0.008
10	0.005	0.005	0.005	0.006	0.008	0.006	0.005	0.005	0.005
11	0.003	0.003	0.003	0.004	0.005	0.004	0.003	0.003	0.003

Supplementary Table 4: Transverse relaxation time (T_2) in μs at different B-field and different temperatures.

Temperature (K)	-20 mT	-15 mT	-10 mT	-5 mT	0 mT	+5 mT	+10 mT	+15 mT	+20 mT
3	607.138	611.257	667.961	793.881	991.274	793.881	667.961	611.257	607.138
4	9.890	10.139	10.775	12.686	15.864	12.686	10.775	10.139	9.890
5	0.817	0.757	0.783	1.050	1.334	1.050	0.783	0.757	0.775
6	0.127	0.155	0.153	0.180	0.231	0.180	0.153	0.155	0.151
7	0.042	0.043	0.042	0.048	0.057	0.048	0.042	0.043	0.042
8	0.017	0.018	0.019	0.022	0.028	0.022	0.019	0.018	0.017
9	0.008	0.008	0.009	0.011	0.014	0.011	0.009	0.008	0.008
10	0.004	0.004	0.005	0.006	0.007	0.006	0.005	0.004	0.004
11	0.002	0.002	0.003	0.003	0.004	0.003	0.003	0.003	0.002

Supplementary Note 4.   ENERGY DEPENDENCE VS ELECTRIC AND MAGNETIC FIELD WITHIN THE 2-QUBIT OPERATING SPACE

A.   Dipolar Couplings, $j_{a,b}^{dip.}(B)$

To understand the origin and evolution of the dipolar coupling between the two HoW_{10} molecules we need to analyze the expectation value of their magnetic moments as they depart from the CT. Indeed, exactly at the CT the neighbours are exactly independent, since they neither experience any first order effect from magnetic field, nor do they themselves create a magnetic field around them. The left panel of Fig. 7 displays a combined information on the electronic and nuclear part of the wavefunction, and can be best understood having Fig. 1 in mind. It can be seen as depicting the derivative of each level in Fig. 1, multiplied by a constant factor, in each case corresponding to M_I.

At high magnetic field approximation, the magnetic moment of Ho spin is saturated and its squared expectation value $\langle J_z \rangle^2$ is 16. Its dipolar coupling, $j_{sat.}^{dip.}$, can be calculated using the well-known equation in cgs units as follows:

$$j_{sat.}^{dip.} = \frac{\mu_B^2}{|r|^3}\left[\bar{g}_a \cdot \bar{g}_b - 3\left(\bar{g}_a \cdot \bar{r}\right)\left(\bar{r}\cdot\right)\bar{g}_b\right] \tag{21}$$

where $\bar{g}_i$ is the corresponding g-tensor, which is obtained from multiconfiguratinoal *ab initio* calculations; $\bar{r}$ is the unit vector at the direction from site a to b and $|r|$ is the length between these two sites. $j_{sat.}^{dip.}$ of -0.0012 cm^{-1} is derived considering the nearest neighbour at distance $|r| = 11.2$ Å. The dipolar coupling at a given magnetic field away from the CT, $j_{a,b}^{dip.}$, is dependent of the B-field and can be expressed by a variant of Eq. 21 as:

$$j_{a,b}^{dip.}(B) = \frac{\langle J_z \rangle_a \cdot \langle J_z \rangle_b}{M_{J,a} \cdot M_{J,b}}\frac{\mu_B^2}{|r|^3}\left[\bar{g}_a \cdot \bar{g}_b - 3\left(\bar{g}_a \cdot \bar{r}\right)\left(\bar{r}\cdot\right)\bar{g}_b\right] \tag{22}$$

where $\langle J_z \rangle$ is the expected angular momentum, which is varied by the B-field and is identical to $M_J = \pm 4$ at high B-field approximation, where the magnetic moment of Ho^{3+} spin is saturated. The right panel of Fig. 7 shows the B-field dependence of the diplolar coupling, which cancels completely at each CT and has a locally square dependence in its vicinity since the dipolar coupling between the two molecules is a direct consequence of their expectation value $\langle J_z \rangle$.
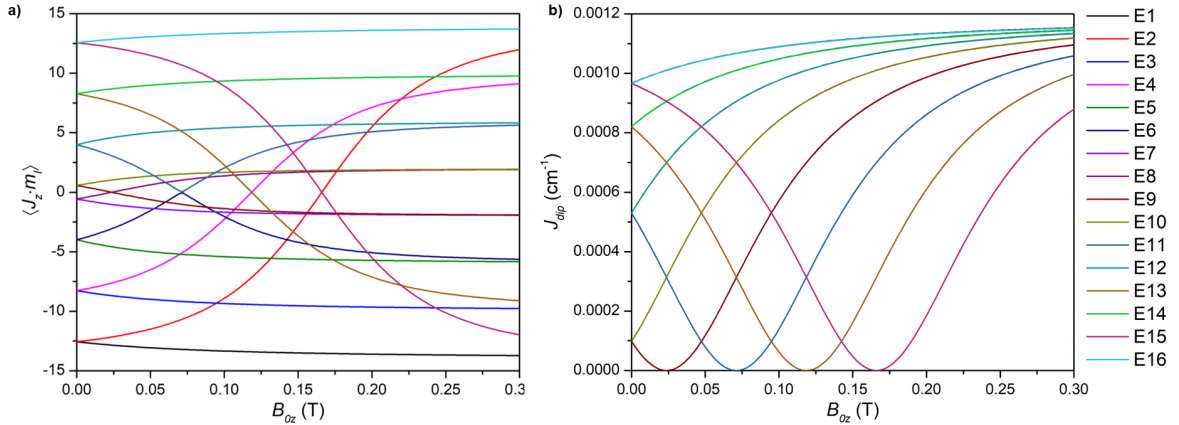

Supplementary Figure 7. a) Expectation Jz values of the 16 spin levels at different magnetic fields for HoW$_{10}$, considering the hyperfine interaction of the ground doublet ($M_J = \pm 4$) with the nuclear spin ($I = 7/2$). b) Calculated dipolar interaction ($j_{a,b}^{dip.}$) of the 16 spin levels of a HoW$_{10}$ molecule with its neighboring molecule in a two-qubit pair.

B.   Energy Level Scheme for Di-nuclear system

Let us first locate the four energy levels that constitute our operating space among the large space of 256 electronu-clear spin states created by a dimer of HoW$_{10}$ molecules, each with a 16 level manifold. As will be seen in more detail in the next Supplementary Section, the natural levels to consider as a 2-qubit operating space are levels 64, 123, 124 and 193. They correspond, in very good approximation, to the four combinations of the ground and excited states of the CT in the two HoW$_{10}$ molecules (ground-ground, ground-excited, excited-ground, excited-excited).

Essentially, the upper and lower levels behave vs the magnetic field as regular CTs, since they can be well approximated as the addition of the CT energies of molecule 1 and molecule 2. In turn, the intermediate levels behave vs the magnetic field as almost perfect diamagnetic systems, since they can be well approximated as the substraction of the CT energies of molecule 1 and molecule 2. The levels are highlighted in Supplementary Figures 8 and 9, with increasingly detailed zooms to allow distinguishing the behaviors of the two intermediate levels and their subtle deviation from perfect diamagnetism. Note that we employed this approximation of two independent molecules only in this text description: all representations correspond to the actual coupled system.
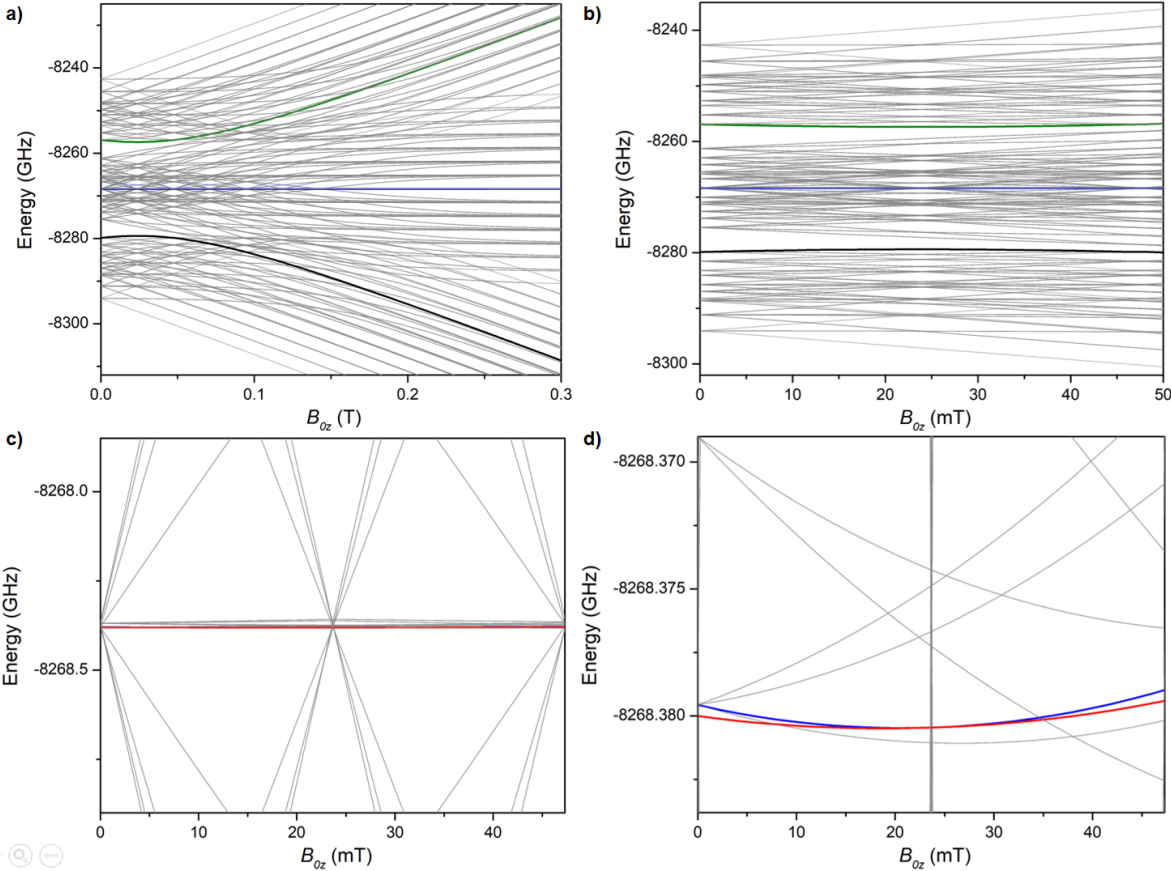
Supplementary Figure 8. a) Spin energy levels evolution of 256 levels for coupled HoW$_{10}$ pair at different magnetic field and at 0 V electric field, and b) its zoomed-in scheme focusing on the vicinity of the first CT. The selected four levels are highlighted as black, red, blue and green for levels 64, 123, 124 and 193, respectively. c) Zoomed-in scheme of the middle 128 levels in b) showing a nearly horizontal behavior upon magnetic fields. d) Zoomed-in scheme of the horizontal levels focusing on levels 123 and 124.
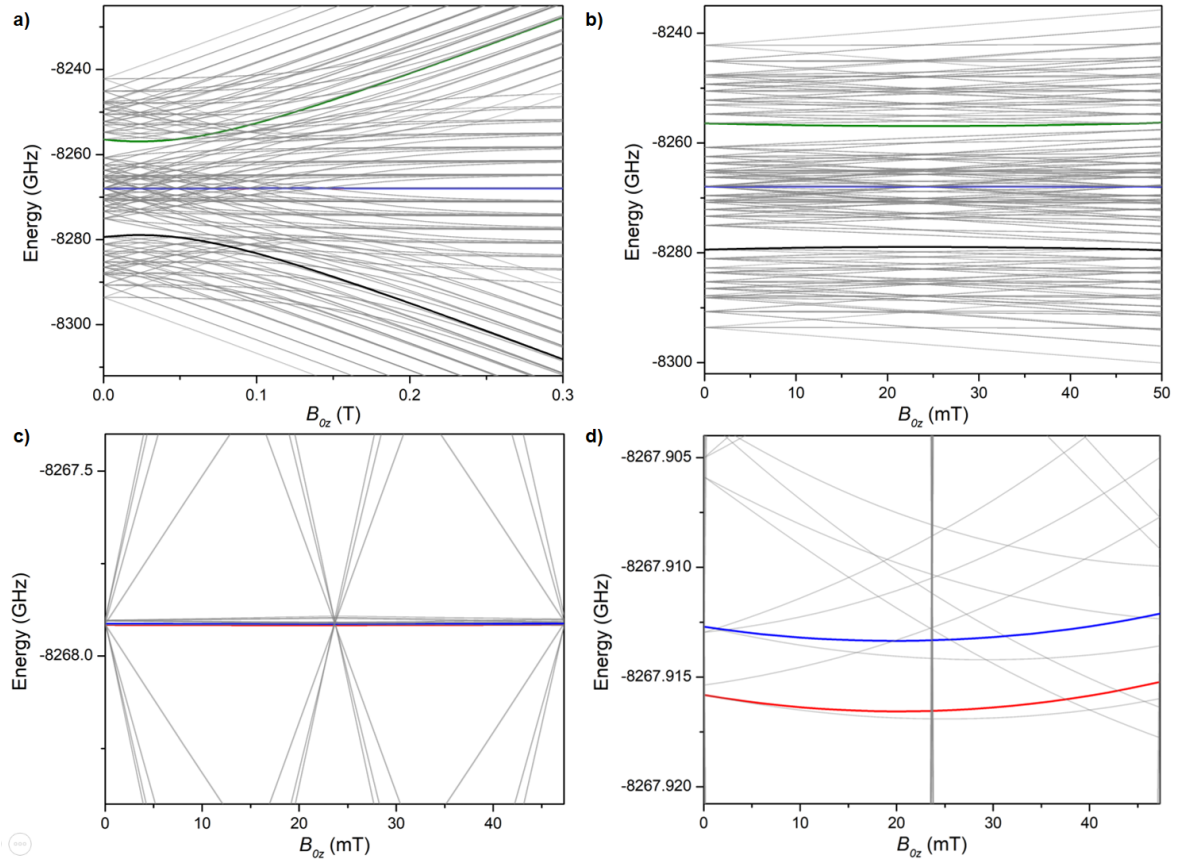
Supplementary Figure 9. a) Spin energy levels evolution of 256 levels for coupled HoW_{10} pair at different magnetic field and at 300 V electric field, and b) its zoomed-in scheme focusing on the vicinity of the first CT. The selected four levels are highlighted as black, red, blue and green for levels 64, 122, 124 and 193, respectively. c) Zoomed-in scheme of the middle 128 levels in b) showing a nearly horizontal behavior upon magnetic fields. d) Zoomed-in scheme of the horizontal levels focusing on levels 122 and 124.

C. Wavefunction composition vs electric and magnetic field within the 2-qubit operating space

Wavefunction information for moderate electric field and moderate deviation from the CT in the composition of the 4 states of our operating space.

Supplementary Table 5: Moduli of the different components of the wavefunctions for coupled HoW$_{10}$ dimer, $|M_{j,a}, M_{j,b}\rangle \otimes |M_I = -1/2\rangle$ of four levels at 24 mT (CT), 18mT, and 12 mT at 0 volts.

Magnetic Field	State number	Energy (GHz)	$|-4_a, -4_b\rangle$	$|-4_a, +4_b\rangle$	$|+4_a, -4_b\rangle$	$|+4_a, +4_b\rangle$
24mT	64	-8279.39	0.252	0.250	0.250	0.248
	123	-8268.38	0.500	0.000	0.000	0.500
	124	-8268.38	0.000	0.500	0.500	0.000
	193	-8257.37	0.248	0.250	0.250	0.252
18mT	64	-8279.42	0.215	0.249	0.249	0.288
	123	-8268.38	0.497	0.003	0.003	0.497
	124	-8268.38	0.000	0.500	0.500	0.000
	193	-8257.34	0.288	0.249	0.249	0.215
12mT	64	-8279.51	0.182	0.245	0.245	0.329
	123	-8268.38	0.489	0.011	0.011	0.489
	124	-8268.38	0.000	0.500	0.500	0.000
	193	-8257.25	0.329	0.245	0.245	0.182

Supplementary Table 6: Moduli of the different components of the wavefunctions for coupled HoW$_{10}$ dimer, $|M_{j,a}, M_{j,b}\rangle \otimes |M_I = -1/2\rangle$ of four levels at 24 mT (CT) and 18 mT at 300 volts. Degeneracy is broken by the electrical field.

Magnetic Field	State number	Energy (GHz)	$|-4_a, -4_b\rangle$	$|-4_a, +4_b\rangle$	$|+4_a, -4_b\rangle$	$|+4_a, +4_b\rangle$
24mT	64	-8278.92	0.252	0.250	0.250	0.248
	122	-8267.92	0.250	0.248	0.252	0.250
	124	-8267.91	0.250	0.252	0.248	0.250
	193	-8256.91	0.248	0.250	0.250	0.252
18mT	64	-8278.95	0.215	0.249	0.249	0.287
	122	-8267.92	0.251	0.286	0.213	0.251
	125	-8267.91	0.247	0.217	0.289	0.247
	193	-8256.88	0.287	0.249	0.249	0.215
12mT	64	-8279.04	0.182	0.245	0.245	0.329
	122	-8267.92	0.253	0.321	0.174	0.253
	126	-8267.91	0.236	0.190	0.337	0.236
	193	-8256.78	0.329	0.245	0.245	0.182

Supplementary Table 7: Complex coefficients of the wavefunctions for coupled HoW$_{10}$ dimer, $|M_{j,a}, M_{j,b}\rangle \otimes |M_I = -1/2\rangle$ of four levels at 24 mT (CT), 18mT and 12 mT at 0 volts.

Magnetic Field	State number	Energy (GHz)	$|-4_a, -4_b\rangle |-1/2\rangle$	$|-4_a, +4_b\rangle |-1/2\rangle$	$|+4_a, -4_b\rangle |-1/2\rangle$	$|+4_a, +4_b\rangle |-1/2\rangle$
24mT	64	-8279.39	0.356 +0.354i	0.252 -0.432i	0.252 -0.432i	-0.480 -0.135i
	123	-8268.38	-0.568 +0.421i	-0.002 -0.002i	-0.002 -0.002i	-0.292 0.644i
	124	-8268.38	0.000	0.362 -0.607i	-0.362 +0.607i	0.000
	193	-8257.37	-0.495 + 0.053i	-0.176 -0.468i	-0.176 -0.468i	0.410 -0.289i
18mT	64	-8279.42	0.462 + 0.038i	-0.085 -0.491i	-0.085 -0.491i	-0.488+0.221i
	123	-8268.38	-0.417 -0.569i	-0.032 +0.040i	-0.032 +0.040i	-0.641 -0.294i
	124	-8268.38	0.000	0.602 -0.370i	-0.602 + 0.370i	0.000
	193	-8257.34	-0.434 -0.316i	0.183 -0.464i	0.183-0.464i	0.460 + 0.056i
12mT	64	-8279.51	-0.355 -0.236i	-0.161 + 0.467i	-0.161 + 0.467i	0.572 +0.045i
	123	-8268.38	-0.638 -0.287i	-0.018 + 0.103i	-0.018 + 0.103i	-0.697 +0.059i
	124	-8268.38	0.000	0.706 -0.037i	-0.706 +0.037i	0.000
	193	-8257.25	0.497 + 0.286i	-0.131 +0.477i	-0.131+ 0.477i	-0.426-0.006i

Supplementary Table 8: Complex coefficients of the wavefunctions for coupled HoW$_{10}$ dimer, $|M_{j,a}, M_{j,b}\rangle \otimes |M_I = -1/2\rangle$ of four levels at 24 mT (CT), 18mT and 12 mT at 300 volts. Degeneracy is broken by the electrical field.

Magnetic Field	State number	Energy (GHz)	$\|-4_a, -4_b\rangle \|-1/2\rangle$	$\|-4_a, +4_b\rangle \|-1/2\rangle$	$\|+4_a, -4_b\rangle \|-1/2\rangle$	$\|+4_a, +4_b\rangle \|-1/2\rangle$
24mT	64	-8278.92	-0.490 -0.109i	0.009 + 0.500i	0.017 +0.500i	0.480-0.133i
	122	-8267.92	0.103 -0.489i	-0.498+0.014i	0.501-0.023i	-0.139-0.480i
	124	-8267.91	0.246 -0.436i	0.483 +0.137i	-0.481 -0.128i	0.011 -0.500i
	193	-8256.91	0.471+0.162i	-0.047+ 0.498i	-0.039+0.498i	-0.495+0.079i
18mT	64	-8278.95	0.447+ 0.125i	0.018 -0.498i	0.009-0.499i	-0.523+0.116i
	122	-8267.92	0.460+0.199i	0.091 -0.526i	-0.071+ 0.456i	0.499 -0.041i
	125	-8267.91	-0.454 -0.201i	0.084-0.458i	-0.088 +0.531i	-0.495+0.036i
	193	-8256.88	-0.490 -0.218i	0.090-0.491i	0.082-0.492i	0.463-0.034i
12mT	64	-8279.04	-0.216+0.368i	0.473 + 0.143i	0.476 +0.135i	0.023-0.573i
	122	-8267.92	0.233 + 0.446i	0.427-0.372i	-0.309+ 0.279i	0.415+0.284i
	126	-8267.91	0.243 +0.421i	-0.316+0.301i	0.414 -0.408i	0.413+ 0.257i
	193	-8256.78	-0.500 -0.281i	0.135 -0.476i	0.127-0.478i	0.426 0.009i

**Supplementary Note 5.   TECHNICAL REQUIREMENTS OF PULSES: INITIALIZATION, 1- AND
2-QUBIT OPERATIONS**

Supplementary Table 9 displays the simple correspondence between physical operations and logical operations. In sum, the only three kinds of physical operations in our proposal are the two single-qubit rotations (implemented by microwave pulses) and a two-qubit rotation (implemented by switching off the E-Field during a specific time). With adequate times and microwave B_1 field intensities corresponding to π EPR pulses, these correspond to Pauli σ_x operations and an adequate time τ corresponds to the SWAP gate, but of course in all cases adjusting the times arbitrary rotation angles can be achieved.

Supplementary Table 9. Gate operations

Operation	pulses
$\sigma_x(1)$	$\hbar\omega_1(\pi)$
$\sigma_x(2)$	$\hbar\omega_2(\pi)$
$SWAP$	E-Field (τ)

Let us now offer some technical details for the qubit register initialization, single qubit rotations and two-qubit operations.
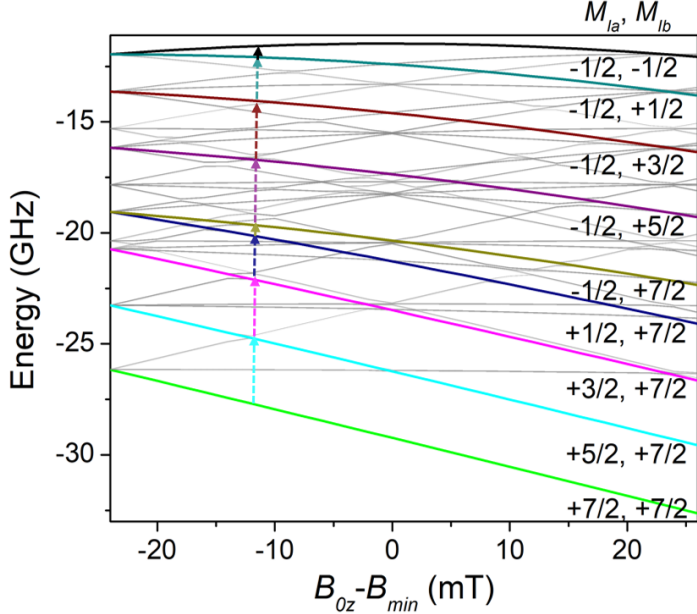
A.   Initialization

This significant level crowding in practice means that in a thermalized system the effective population to start the quantum manipulation will be significantly smaller in experiments targeting pairs of molecules than for individual molecules. The simplest way of improving this is via a moderate cooling, from $T = 5$ K to $T = 3$ K or below. The thermal population of states can be estimated via a Boltzmann distribution, see Supplementary Table 10. This strategy has limitations, in the sense that cooling down to a significantly lower temperature, to the order of 50 mK, removes all population from the operating space.

Supplementary Table 10. Percentage populations of the states of interests at different temperatures at CT (0.024mT) with 0 volt, for the bimolecular system.

State number	ΔE (GHz)	0.05 K	1 K	2 K	5 K
1	0	79.752	1.268	0.740	0.511
64	17.76175	0.000	0.541	0.483	0.431
123	28.76909	0.000	0.319	0.371	0.387
124	28.76909	0.000	0.319	0.371	0.387
193	39.77642	0.000	0.188	0.285	0.349

While in principle it is optional, the proposed initialization sequence is expected to increase the signal-to-noise ratio and thus is desirable in this case. It consists in a series of 8 π pulses that transfer population from a $(+7/2,+7/2)$ nuclear spin state to a $(-1/2,-1/2)$ nuclear spin state via allowed $\Delta M_I = \pm 1$ transitions. The exact transition energy depends on the applied magnetic field. At 12mT away from the CT, the sequence consists in the following frequencies (in GHz): 2.95, 2.66, 1.96, 0.48, 2.94, 2.65, 1.96, and 0.48, as seen in Fig. 3d in the main text.

For the best results in a given diluted crystal, one could apply quantum optimal control to choose the initialization pulse sequence that maximizes the (T_2-weighted) amplitudes of the echos within the operating space[9].

Supplementary Figure 10. Initialization scheme showing the population transfer from the ground level (green) to the first operating level (black) by using 8 consecutive π pulses.

B. Single qubit rotations

In presence of an electric field, the transition energy for qubit 1 is higher than for qubit 2. In both cases, the transition frequency resulting from our calculations is approximately 11.00 GHz (from the experiment, we know this to be approximately 9.15 GHz at the CT). For an electrical field of 150 V/2mm that affects the two molecules in opposite ways (or, in our calculations an electrical field of 300 V/2mm affecting one of the molecules, with respect to a case with no electric field), this generates a shift of about 3 MHz (Supplementary Figure 11). Experimentally, selective addressing has already proven to be achievable in this system under an external electric field of 300V/2mm affecting the two molecules in opposite ways. This requires soft pulses of at least a duration of 400 ns for $\pi/2$ and 800 ns for π pulses.

The length of the pulses, adjusted for the intensity of the B_1 magnetic component of the microwave pulse, will allow to obtain any desired rotation angle.

C. Two-qubit operations

The only two-qubit operation that is straightforward in the present scheme is the SWAP operation. More exactly, any desired rotation between the $|01\rangle$ and $|10\rangle$ states can be achieved by choosing the time of the operation, including the notable $\sqrt{SWAP}$ that together with single-qubit rotations forms a universal gate set. Any other operations need to be constructed from combination of these straightforward gates.

As explained in the text, the SWAP operation starts as soon as the E field is turned off, and can be viewed as a kind of "anti-pulse": it is the absence of E field that makes the two qubits indistinguishable, and this change in the set of the Hamiltonian eigenstates triggers the rotation. The typical times will be given by the inverse of the interaction energy between the two molecular spins. At 12 mT away from a CT, this interaction is in the order of 0.1 MHz (Figure 3c in main text, black line), meaning a full rotation would take in the order of 10 μs. This is comparable to the T_2 value at 5 K, but conveniently below the estimated T_2 times at 3 or even 4 K, meaning any cooling below 5 K would suffice.
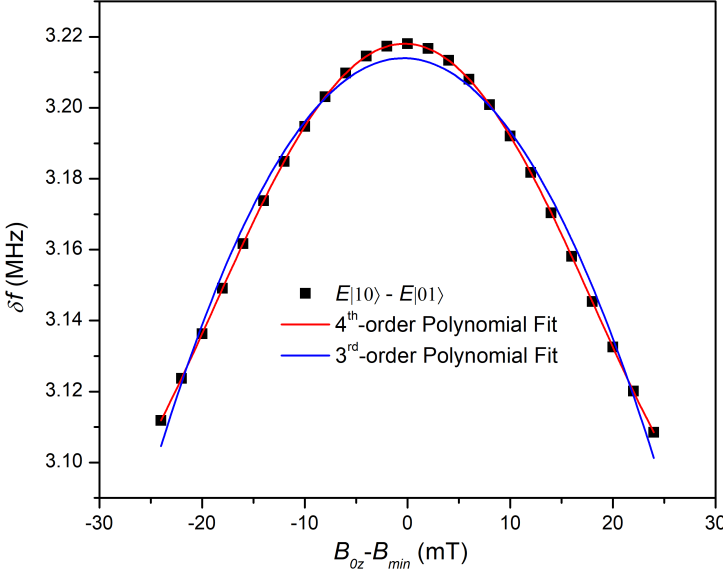
Supplementary Figure 11. δf as a function of the $B-$field in the presence of an $E-$field of 300 V, and its best 3rd and 4th order polynomial fits. The 4th order polynomial fit returns to a 3rd order protection from magnetic noise (a 3rd-order CT).

Supplementary Note 6.   STRATEGIES TO DEAL WITH LIMITATIONS OF THE PROPOSAL

As indicated in the main text, operating dimers within a diamagnetically diluted crystal involves a crucial technical difficulty, namely dealing with the signal from monomers, which will be statistically more abundant. In the example operation discussed in the main text, which generates the superposition $\Phi_{14}^{\pm} = \frac{1}{\sqrt{2}}(|00\rangle \pm |11\rangle)$ the signal of the monomers is naturally suppressed, since they experience a full 2π rotation.

Interestingly, this is not an isolated case. For different quantum operations, it is possible to translate the desired sequence into one that also cancels out any excitations of the monomers, i.e. for both transition energies the total rotation must be a multiple of 2π, and any Hadamard gate needs to be canceled out. For example, the quantum circuits depicted in Fig. 12, obtained by using the online simulator quirk at https://algassert.com/quirk , show how different coherent superpositions of two qubits, (symmetric or asymmetric) can be achieved by pulse sequences that can be trivially shown to have no effect on isolated qubits.

Another experimental limitation of the proposed scheme derives from the low symmetry of the crystal structure. In contrast to simpler solids, in this molecular crystal there is a mismatch between the idealized D_{4d} (or even C_4) symmetry of the single molecule and the number of countercations (9), determined by the charge. This causes every one of the nearest neighbours from a molecule in the crystal to be distinct, both in terms of distance and relative orientation. In practice, this means that in a real diluted sample there will not be a unique dipolar coupling between pairs of HoW$_{10}$ neighbours, but instead a distribution of couplings. Indeed, in the crystal if one focuses on a "central" HoW$_{10}$ molecule there are in the order of 20 possible non-equivalent near-neighbours at comparable distances around, and of course an infinity more at larger distances. Half of the neighbours will have the same orientation as the central molecule, with the other half presenting an inversion-related orientation. This means (a) in 50% of the cases, neighbouring pairs will not be distinguishable by means of an electric field, with the result being that this part of the protocol will fail for those pairs of molecules and (b) throughout the sample there will be a spread of dipolar coupling values, both in magnitude and in sign. For the experiment, this means that the duration of the electric field pulse will need to be empirically adjusted to maximize the echo.

A further, related, real-world limitation of the stability of this highly protected qubit are local electric fields caused by the crystal environment. Any electric fields caused by a crystalline defect and felt by the qubit molecules, e.g. a Na$^+$ vacancy in the vicinity of one of the HoW$_{10}$ molecules, will have the same qualitative effect as the external electric field pulse, i.e. break the symmetry between the two HoW$_{10}$ entities and cause an alteration in the expected spin dynamics. Empirically, different crystallization procedures can be tested to address this.
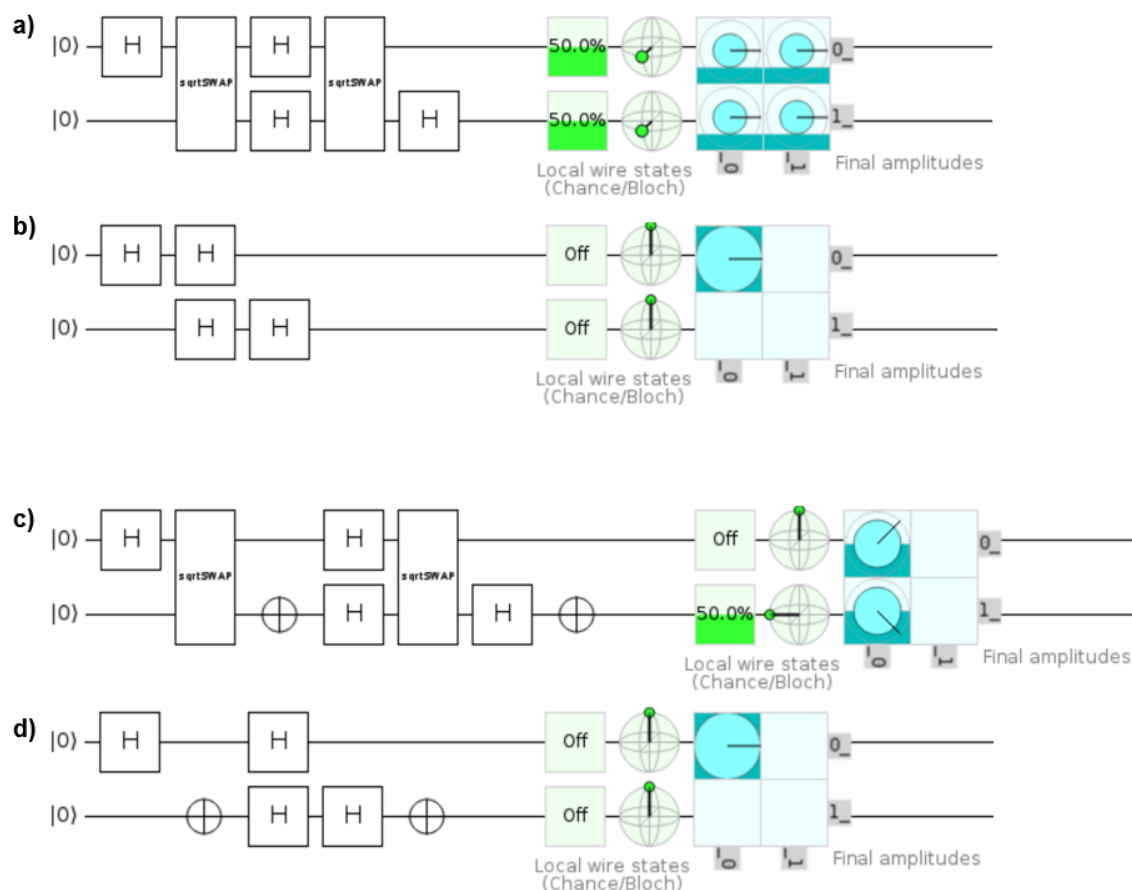
Supplementary Figure 12. a) Sequence of logical operations that generate an entangled state involving $|00\rangle, |01\rangle, |10\rangle, |11\rangle$. b) Same sequence, but omitting the effect of the 2-qubit gates, produces no net effect on the single qubits. c) Sequence of logical operations that generate an entangled state involving $|00\rangle, |01\rangle$. b) Same sequence, but omitting the effect of the 2-qubit gates, produces no net effect on the single qubits.

SUPPLEMENTARY REFERENCES

[1] Shiddiq, M. *et al.* Enhancing coherence in molecular spin qubits via atomic clock transitions. *Nature* **531**, 348–351 (2016).

[2] Gatteschi, D., Sessoli, R. & Villain, J. *Molecular nanomagnets*, vol. 5 (Oxford University Press, 2006).

[3] Orbach, R. Spin-lattice relaxation in rare-earth salts. *Proceedings of the Royal Society of London. Series A. Mathematical and Physical Sciences* **264**, 458–484 (1961).

[4] Blockmon, A. L. *et al.* Spectroscopic analysis of vibronic relaxation pathways in molecular spin qubit [ho (w5o18) 2] 9–: Sparse spectra are key. *Inorg. Chem.* **60**, 14096–14104 (2021).

[5] Lunghi, A., Totti, F., Sessoli, R. & Sanvito, S. The role of anharmonic phonons in under-barrier spin relaxation of single molecule magnets. *Nat. Commun.* **8**, 1–7 (2017).

[6] Lunghi, A. & Sanvito, S. The limit of spin lifetime in solid-state electronic spins. *J. Phys. Chem. Lett.* **11**, 6273–6278 (2020).

[7] Briganti, M. *et al.* A complete ab initio view of orbach and raman spin–lattice relaxation in a dysprosium coordination compound. *J. Am. Chem. Soc.* **143**, 13633–13645 (2021).

[8] Lunghi, A. Toward exact predictions of spin-phonon relaxation times: An ab initio implementation of open quantum systems theory. *Sci. Adv.* **8**, eabn7880 (2022).

[9] Spindler, P. E., Schops, P., Kallies, W., Glaser, S. J. & Prisner, T. F. Perspectives of shaped pulses for epr spectroscopy. *J. Magn. Reson.* **280**, 30–45 (2017).